Journal of the Optical Society of America A
OPTICS, IMAGE SCIENCE, AND VISION

How to efficiently characterize special effect coatings

CHRISTIAN STROTHKÄMPER,* KAI-OLAF HAUER, AND ANDREAS HÖPE†

Physikalisch-Technische Bundesanstalt, Bundesallee 100, 38116 Braunschweig, Germany
**Corresponding author: christian.strothkaemper@ptb.de*

Received 5 June 2015; revised 2 November 2015; accepted 2 November 2015; posted 3 November 2015 (Doc. ID 242504); published 3 December 2015

Coatings and plastics that contain special effect pigments show angular-dependent reflection characteristics. Interference pigments, for instance, exhibit a color impression ("appearance") that changes with the directions of illumination and observation. It is currently an open question how the appearance of such coatings can be best characterized without extensive measurements of the spectral radiance factor. In this paper, a simple and efficient approach is presented on how to characterize the appearance of surfaces composed of metallic and interference pigments. Based on the rotational symmetry of the pigment distribution around the surface normal, it is demonstrated how the appearance at any configuration of illumination and observation can be estimated from a set of in-plane measurements. For practical applications, it is shown that a rather small number of geometries (e.g., 10) are sufficient. The presented methodology is an alternative to a recent principal components analysis-based procedure and offers the advantage of being based directly on an extensible physical model while having at least the same prediction accuracy. © 2015 Optical Society of America

OCIS codes: (120.3940) Metrology; (290.1483) BSDF, BRDF, and BTDF; (330.1710) Color, measurement; (330.1720) Color vision; (330.1730) Colorimetry.

http://dx.doi.org/10.1364/JOSAA.33.000001

1. INTRODUCTION

Coatings and plastics that contain effect pigments enable manufacturers to equip their products with eye-catching appearance effects [1–3], as can be seen in Fig. 1. Different types of effect pigments are commercially available, for instance, metallic pigments, interference pigments and diffraction pigments. In this study, we focus on metallic and interference pigments. Metallic effect pigments are mostly aluminum micro-platelets specularly reflecting the incident light. The visual effect of these micromirrors for an observer is a glittering appearance of the surface [4]. Extended possibilities are offered by interference pigments and diffraction pigments [2,5]. Interference pigments are also micro-platelets consisting of a layered structure of semi-transparent materials with different refractive indices. The reflectance spectrum of this layered structure is determined by the layer thicknesses, their refractive indices and the angle of incidence [6]. So by tailoring thickness and composition of the layers, manufacturers can tune the goniochromatic appearance of interference pigments.

The pigments themselves are randomly dispersed in the coating regarding their position and, within certain limits, also with respect to their angle with the surface normal. Hence, for a given observing direction, the impinging light on the surface is reflected on a subset of pigments which are suitably oriented. Respectively, directional incoming light is distributed in a certain range of directions by the effect pigments, which is, however, not as large as in diffuse scattering.

The hue, chroma, and lightness of the perceived luminance of special effect coatings change with visual perspective and ambient lighting conditions, so they pose a challenge for metrology. In principle, a complete characterization of the appearance can be achieved by exhaustive sampling of the spectral radiance factor for different illumination and observation geometries, i.e., in four angular dimensions, which is not a practical option. Finding efficient ways to characterize the appearance of goniochromatic surfaces is thus an emerging and important topic especially for industrial applications but also for computer graphics [7,8].

Commercial color-measuring instruments based on existing standards [9–11] and recommendations [12] are not capable of fully characterizing the goniochromatic appearance because of the limited number of standardized geometries and hence, a set of optimal measurement geometries is not yet generally established. However, recent progress in the characterization of special effect coatings was made by noticing the importance of flake-based parameters [13–19], i.e., making use of the flake incident angle γ on the pigments and their inclination angle δ relative to the sample surface (Fig. 2).



Fig. 1. Roadster with a special effect coating based on interference pigments, producing a colorful appearance of the reflected light in various spatial directions.

As pointed out by Kirchner and Cramer [12], the flake incidence angle γ determines the pigments' spectral reflectance and this important quantity should be sampled at illumination/detection configurations where γ but not δ is varied in order to obtain information on the hue [18]. Similarly, as stressed by Rösler *et al.* [13], the amount of pigments on which the light is reflected in a given illumination/detection configuration depends on the distribution of the inclination angle δ because pigments that are strongly tilted are not as common as those that are only slightly tilted. The effect of this angular distribution on chroma and lightness is proposed to be best probed by choosing measurement geometries where δ is varied while γ is kept constant [18].

Ferrero *et al.* utilized the approach that a part of the appearance of effect pigmented samples is proportional to the distribution function of the inclination angle δ and the pigment's angular dependent spectral reflectance $R(\lambda, \gamma)$. They derived a formalism to deduce the spectral radiance factor—and thus the appearance—of special effect coatings at any geometry from a small set of measured geometries (about a number of 10) [15,18]. Their approach is based on a principal component analysis (PCA) of the measured spectra, where the four most important eigenspectra are used to predict the appearance at other geometries. This is done by modeling the angular dependence of the eigenvalues. However, this methodology has the drawback of not being based on a physical model.

In the following an alternate approach is presented to predict the $L^*a^*b^*$ color coordinates [20] of effect pigmented

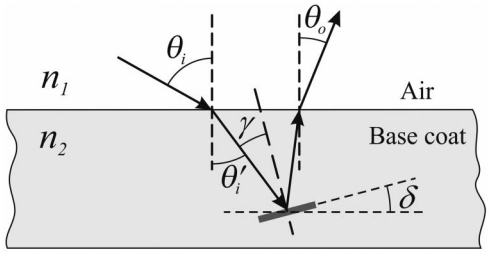

Fig. 2. Definition and relationship of the polar angles θ_i and θ_o, which describe the angles of incident light and the observer relative to the surface normal, and the flake incidence angle γ and inclination angle δ.

Table 1. Samples Used in This Study

Sample ID	Effect Pigment (Product Name)
CF	Chromaflair Green/Purple 190L
MB	Miraval 5424 Magic Blue
LS	Colorstream T20-04 WNT Lapis Sunlight
SH	Stapa Hydrolan 8154
VF	Colorstream T20-01 WNT Viola Fantasy
SR	Xirallic T60-21 SW Solaris Red

samples for any spatial configuration of light source and observer from a set of as few as 10 measured in-plane geometries, i.e., geometries where the radiance is measured in the plane of incidence. The approach is based on the idea of Ferrero *et al.* [15,18] that the appearance is largely influenced by the pigments' angular distribution and the angular dependence of the spectral reflectance. However, it does not rely on the PCA formalism to separate spectral and geometrical information. Rather, the tristimulus values [21], which already represent a massive compression of the spectral data, are directly related to a physical model, which offers the additional benefit of being adaptable and extensible.

2. MATERIALS AND METHODS

A. Samples

The samples within this work consist of a set of six metal sheets, covered by coatings containing different effect pigments (Table 1). The sheets were first primed with a black background. Then, except for sample SR, a base coat with the effect pigments and subsequently a clear coat were applied. Sample SR with Xirallic Solaris Red pigments has two base coat layers. One contains the effect pigments, while the other below contains blue absorption pigments.

Figure 3 exemplifies the visual appearance of the samples under direct sunlight. A granular structure can be observed in all cases because the picture is composed of many microreflections [22,23]. The samples CF, MB, LS and VF are representatives of goniochromatic coatings based on interference pigments where the $L^*a^*b^*$ color space values exhibit large variations. Sample SH is a representative of an achromatic metallic

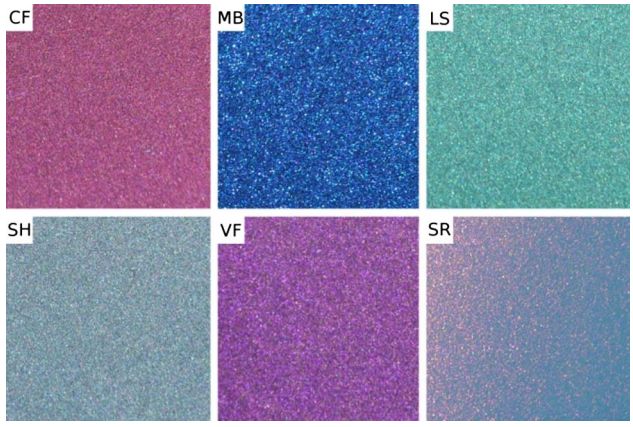

Fig. 3. Photographs of the six samples of this study taken under direct sunlight (cf. Table 1). Each picture shows an area of about 4 cm^2.

paint containing cornflake shaped aluminum pigments showing strong variations in L^* while a^* and b^* are about zero. Sample SR is included in this study to test the applicability of the presented model for applications where an effect pigment is combined with conventional absorptive pigments.

B. Goniochromatic Measurements

The measurements were performed with the ARGon[3] goniorefelectometer facility at PTB, which has been described in detail recently [24]. In brief, a special light source based on a halogen lamp with a spatially homogenous beam profile is set up on a ring mount so that it can be rotated around the sample. The sample is mounted on a robot arm in the center of the ring mount. Light reflected or scattered from the sample is detected by a stationary imaging system. Since the robot arm can position the sample in any spatial orientation and the light source can be rotated around the robot arm, nearly any directional configuration of incident light and observation with respect to the sample surface can be realized.

We use a polar coordinate system with a polar angle θ and an azimuthal angle φ (cf. Fig. 4) to describe the directions of illumination (θ_i, φ_i) and observation (θ_o, φ_o). So, for instance, an in-plane geometry with industrial nomenclature of 45as15 is described by $(\theta_i, \varphi_i, \theta_o, \varphi_o) = (45°, 0°, 30°, 180°) = (45°, 0°, -30°, 0°)$.

Four geometries were chosen for the incident light (azimuthal angle of $\varphi_i = 0°$ and four different polar angles θ_i: 0°, 22.5°, 45° and 67.5°). At each illumination angle, the radiance of the sample is measured on a grid over a quarter sphere, as depicted in Fig. 4, where the azimuthal angle ranges from 0° to 180° and the polar angle θ_o ranges from 0° to 70°. The result of the measurement is the spectral radiance factor $\beta(\theta_i, \varphi_i, \theta_o, \varphi_o, \lambda)$, which is simply the quotient of the samples spectral radiance to the radiance of the perfectly reflecting diffuser (PRD),

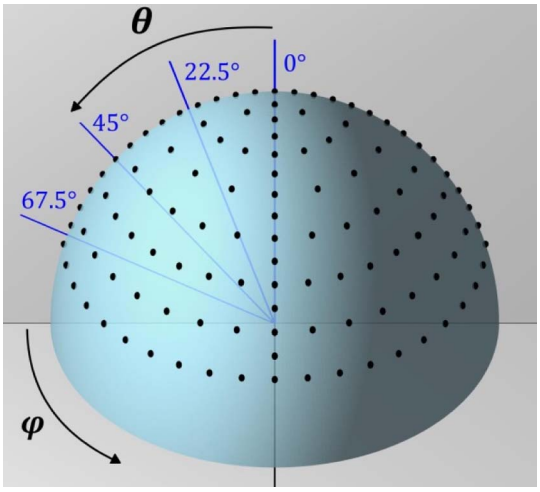

Fig. 4. Illustration of the measurement geometries with four different illumination angles of 0°, 22.5°, 45° and 67.5° and a total of 110 directions under which the spectral radiance from the sample is observed (black dots). The observing directions are distributed over a quarter sphere, which is bordered by the plane of incidence and the sample surface. For each illumination angle, there are certain geometries that are not realized, e.g., retroreflection (see Fig. 5 for details).

$$\beta(\theta_i, \varphi_i, \theta_o, \varphi_o, \lambda) = \frac{L_r(\theta_i, \varphi_i, \theta_o, \varphi_o, \lambda)}{L^{\mathrm{PRD}}}. \quad (1)$$

Since the appearance of the samples in this study is practically invariant when light source and observer are rotated around the sample normal, $\beta = \beta(\theta_i, \theta_o, \varphi_o - \varphi_i, \lambda)$, it is no restriction to set $\varphi_i = 0$. The appearance is also practically mirror symmetrical with regard to the plane of incidence. Hence $\beta(\varphi_o - \varphi_i) = \beta(\varphi_i - \varphi_o)$ and it is thus no restriction to limit ϕ_o to 180°.

C. Flake-Based Angles

Due to the different refraction indices of air ($n_1 \cong 1$) and the base coat ($n_2 \approx 1.5$), light that enters and leaves the coating layer is refracted at the interface (Fig. 2). Because of the refraction and the generally nonzero flake inclination angle δ, the flake incidence angle γ is generally different from the angle of incidence θ_i on the base coat.

The directional angles of the incident light (θ_i', φ_i') and the observer (θ_o', φ_o') inside the coating layer,

$$\sin\theta_{i,o}' = \frac{n_1}{n_2}\sin\theta_{i,o},$$
$$\varphi_{i,o}' = \varphi_{i,o}, \quad (2)$$

define a number of pigments $N(\delta)$ that are suitably orientated to enable specular reflection. The inclination angle δ and incidence angle γ of this set of pigments are uniquely determined by [17]

$$\cos 2\gamma = \sin\theta_i'\sin\theta_o'\cos\varphi_o + \cos\theta_i'\cos\theta_o',$$
$$\cos\delta = \frac{\cos\theta_i' + \cos\theta_o'}{\sqrt{2 + 2\cos 2\gamma}}. \quad (3)$$

Conversely, the solution of the reverse equations is not unique but rather defines isochromatic lines, where the appearance is approximately invariant [19].

In the most general case, the angular distribution function $N(\delta)$ of the pigments would also depend on the azimuthal angle [25]. However, a rotational anisotropy is generally not desired by manufacturers and hence not practically realized. Therefore $N = N(\delta)$ is a reasonable approximation and used in the following.

3. SEPARATING CHROMA AND HUE

Figure 5 shows the values of the flake-based parameters δ and γ that belong to the measurement geometries depicted in Fig. 4 according to Eq. (3). It can directly be seen how the area in the δ-γ plane changes its shape and size when the illumination angle is varied and the center of mass shifts away from the origin.

The vertical and horizontal lines in Fig. 5, defined by $\delta_0 = 2.3°$ and $\gamma_0 = 2.3°$, respectively, border the area of measurement geometries that are evaluated here. Due to spatial restrictions, the minimal angle between illumination and observation is 7°, which translates into 4.6° inside the coating and thus $\gamma > 2.3°$. To avoid any light directly reflected on the base coat, a lower limit of 7° was also chosen for the angle between observation and the specular reflection on the base coat, which means $\delta > 2.3°$. Due to the finite (angular) aperture and the slightly uneven sample surface, specular reflections at the

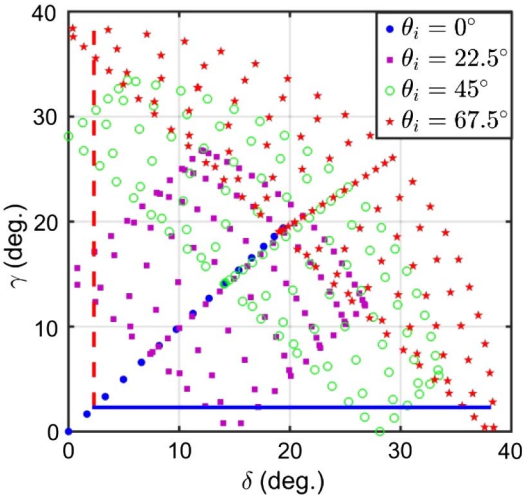

Fig. 5. Scatter plot of the flake inclination angle δ and the flake incidence angle γ that correspond to the geometries in Fig. 4 via Eq. (3). Geometries to the left of the vertical line and below the horizontal line are disregarded for reasons described in the text. Measurements of the appearance at several geometries along the vertical and horizontal lines are used for the global color prediction.

air/coat interface would otherwise influence the measured data. However, specular reflections are not the focus of this paper because they are essentially characterized by the spectrum of the incident light and dominate the appearance in geometries where they occur.

Keeping the flake inclination fixed while sampling the flake incidence angle γ, i.e., measuring on a vertical line in Fig. 5, allows for probing the hue range as demonstrated in Fig. 6. It can also be seen that measuring at a constant flake incidence angle is a way to probe the chroma with almost no variation in hue. The measurement configurations that are bordered by the lines in Fig. 5 have color coordinates that are bordered by the color coordinates measured along these lines. So by choosing δ_0 and γ_0 as small as possible for a given experimental setup, the volume of the color space of a sample in terms of hue and chroma can be optimally probed.

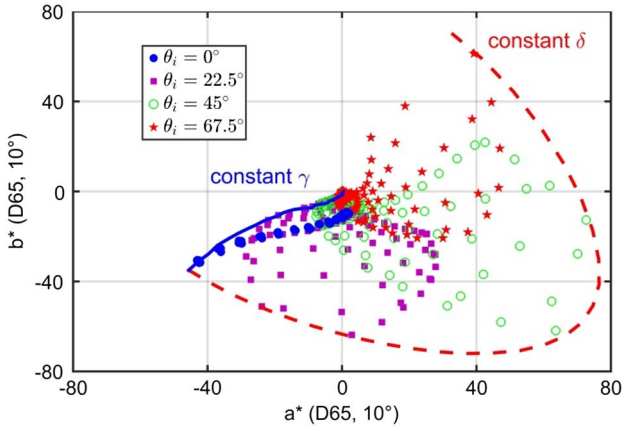

Fig. 6. Measured a^*b^* color coordinates of sample CF. The solid and dashed lines point out the color coordinates that are measured on the horizontal and vertical lines, respectively, in Fig. 5.

As demonstrated in Fig. 6, separating δ and γ is essentially a way to separate variations in the appearance into chroma and hue. This is an advantage over the recently proposed "interference lines" [17] and "absorption lines" [14], which are sets of in-plane geometries defined for a constant value of $\theta_i + \theta_o$ and $\theta_i - \theta_o$, respectively. These two lines are easily defined but they generally mix chroma and hue. This mixing is even stronger for the often used "aspecular line" (defined by a constant θ_i), where the mixing would even occur if there was no refraction at the air/coating interface. On the other hand, separating chroma and hue necessitates the use of nonconstant sets of measurement geometries that have to be adapted if a base coat with an untypical refractive index shall be used. However, it will be shown in the following that this effort may be worthwhile because it allows for a rather straightforward appearance prediction.

4. MODELING THE APPEARANCE

To model the appearance it is assumed that the observed light can be divided into two components, a specular one and a diffuse one (Fig. 7) [7,8]. The specular component originates in rays of light that reach the observer via specular reflection (which includes possible interference effects [3]) on a single flake pigment, while all other processes such as scattering (b) and multiple reflection on flakes (c) are subsumed in the diffuse component.

Upon hitting the air/clear coat interface, a part of the incident light is specularly reflected while a fraction,

$$T_1(\theta_i, \theta_i') = \frac{1}{2}\left[\frac{4n_2 \cos\theta_i'}{\left(1+\frac{n_2\cos\theta_i'}{n_1\cos\theta_i}\right)^2} + \frac{4n_1\cos\theta_i'}{\left(1+\frac{n_1\cos\theta_i'}{n_2\cos\theta_i}\right)^2}\right], \quad (4)$$

is transmitted into the coat, as follows from the Fresnel equations [6]. Equation (4) is the average of the transmittance of light polarized perpendicular and parallel, which is valid for the unpolarized light of the irradiating lamp used in the given setup. The transmittance T_2 of light directed back from the coat into air is also given by Eq. (4) interchanging the subscripts of i and o.

Considering the processes illustrated in Fig. 7, a very basic assumption to model the spectral radiance factor β is the following:

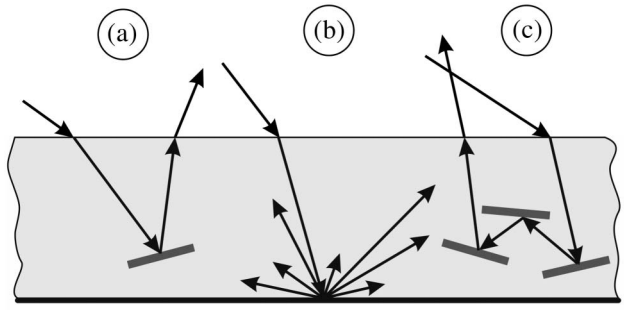

Fig. 7. Main processes that occur for a ray of light in the coating are (a) specular reflection on a single pigment, (b) scattering, e.g., at the substrate or at the edges of the pigment flakes, and (c) specular reflection on multiple pigments.

$$\beta \propto T_1 A(\delta) R(\lambda, \gamma) T_2 + T_1 S(\lambda, \theta_i', \varphi_i', \theta_o', \varphi_o') T_2. \quad (5)$$

The first part, as illustrated by process (a) in Fig. 7, describes specular reflection on a number of suitably oriented pigments $N(\delta)$ that have a reflectance $R(\lambda, \gamma)$. This ensemble of pigments has an average pigment area $a(\delta)$ that depends on the flake inclination because larger pigments may be less tilted on average [13], so that the combined area of the ensemble is $A(\delta) = N(\delta)a(\delta)$. With the approach that is pursued in the following it will not be necessary to derive an explicit, analytical expression for $R(\lambda, \gamma)$ or $N(\delta)$ and $a(\delta)$. However, $N(\delta)$ can be expected to resemble a Gaussian distribution [13] and it will turn out in the next section that $-\log(A(\delta)) \propto \delta$. Any other processes, such as diffuse reflectance at the substrate or successive reflection at multiple, differently tilted pigments (processes (b) and (c) in Fig. 7), which may also include total reflexion at the base coat/air interface, are described by $S(\lambda, \theta_i', \varphi_i', \theta_r', \varphi_r')$. Modeling this part is challenging but here the admittedly rather rough approximation is made that it is independent on any angle

$$S(\lambda, \theta_i', \varphi_i', \theta_r', \varphi_r') \equiv S(\lambda). \quad (6)$$

So the total radiance of all processes other than the specular reflection on a set of pigments with equal orientation is taken to be proportional to the radiance of the perfectly diffusing reflector [26].

The X, Y, Z tristimulus values [21], from which the $L^*a^*b^*$ color coordinates are calculated [20], follow from the spectral radiance factor as

$$\begin{bmatrix} X \\ Y \\ Z \end{bmatrix} = \frac{100}{\int \bar{y}(\lambda) I(\lambda) \mathrm{d}\lambda} \int \beta(\lambda) \begin{bmatrix} \bar{x}(\lambda) \\ \bar{y}(\lambda) \\ \bar{z}(\lambda) \end{bmatrix} I(\lambda) \mathrm{d}\lambda. \quad (7)$$

Here, $\bar{x}, \bar{y}, \bar{z}$ are the CIE color matching functions [21] and $I(\lambda)$ is the spectral power distribution of the illuminant for which the color appearance shall be derived.

The illuminant is chosen as D65 [27] (representative for daylight), because of its huge relevance, e.g., in all outdoor and automotive applications. The dispersion of the base coat in the visible optical range is small and using $n_2 = 1.5$, it is neglected. Hence, the spectral dependence of T_1 and T_2 does not have to be taken into account and it follows from Eqs. (5) and (7) that X, Y, Z can each be decomposed into a specular component and a diffuse component, e.g., $X(\delta, \gamma) = X_s + X_d$ with

$$X_s(\delta, \gamma) = T_1 T_2 A(\delta) R_X(\gamma),$$
$$X_d = T_1 T_2 X_0, \quad (8)$$

where $R_X(Y) \propto \int R(\lambda, \gamma) x(\lambda) I(\lambda) \mathrm{d}\lambda$ and $X_0 \propto S(\lambda) x(\lambda) I(\lambda)$. Here and in the following, if something is discussed exemplarily for one of the tristimulus values, e.g., X, it likewise applies to the other tristimulus values, e.g., Y and Z.

Due to the assumption of specular reflection on the pigments in Eq. (5), the present methodology can be applied to metallic and interference pigments but not to, e.g., diffracting pigments.

5. TESTING THE MODEL

Figure 8 exhibits the tristimulus values of the samples CF and SH in geometries where once the inclination angle and once the flake incidence angle is kept constant (cf. the vertical and horizontal lines, respectively, in Fig. 5). Comparing Figs. 8(a) and 8(b) makes very evident that the angular dependence of the tristimulus values as a function of either δ or γ is essentially the same in the case of metallic pigments but not so in the case of interference pigments. The reason for this is that the spectral radiance factor of metallic pigments shows very little variation in the visible.

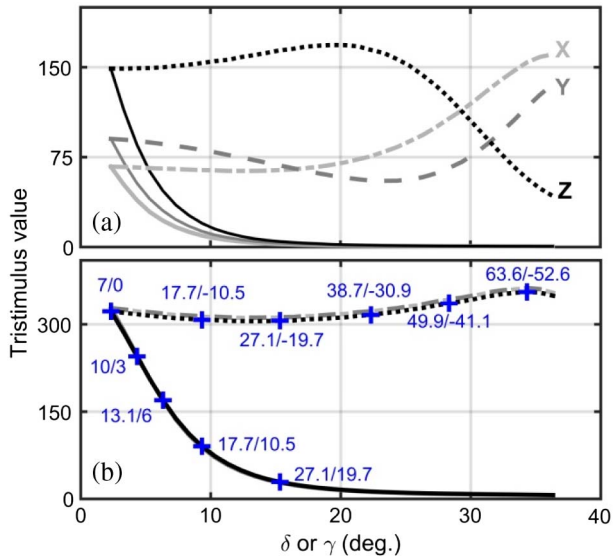

Fig. 8. X, Y and Z tristimulus values of the samples (a) CF and (b) SH measured as a function of (δ_0, γ) at constant inclination angle (broken lines) and as a function of (δ, γ_0) at constant flake incidence angle (solid lines). The symbols point out a set of only 10 geometries, which is tested as a practically relevant basis for color prediction. These geometries are labeled in θ_i/θ_o format.

At a constant flake incidence angle, the tristimulus values, e.g., $X(\delta, \gamma_0)$, decrease roughly exponentially with increasing inclination angle. This is exactly what would be expected if Eq. (8) can be applied because $X(\delta, \gamma_0)$ is mainly determined by $A(\delta)$ and very few pigments will be strongly inclined [13]. However, if the inclination angle is kept constant, then the tristimulus values, e.g., $X(\delta_0, \gamma)$, exhibit an oscillatory behavior (here $\delta_0 = \gamma_0 = 2.3°$). This can also be understood with Eq. (8) because $X(\delta_0, \gamma)$ is mainly determined by $R_X(\gamma)$. Figure 8 suggests that the diffusive component can be obtained for high values of δ where $A(\delta)$ is essentially zero. So, for instance, $X_d = \mathrm{X}(30°, \gamma_0)$.

The tristimulus values as a function of (δ, γ_0) and (δ_0, γ), such as the data shown in Fig. 8, serve as the basis for the appearance prediction at any geometry (δ, γ). For this purpose, the tristimulus values are sampled along the lines in Fig. 5 using the two cases of a dense sampling with 1° spacing and a total of 70 geometries and a sparse sampling where only 10 geometries are used, which are detailed in Figs. 8 and 9.

The tristimulus values are scaled as

$$\frac{X(\delta, \gamma_0) - X_d}{T_1 T_2} = A(\delta) R_X(\gamma_0) := f(\delta) \quad (9)$$

and

$$\frac{X(\delta_0, \gamma) - X_d}{T_1 T_2} = A(\delta_0) R_X(\gamma) := g(\gamma) \quad (10)$$

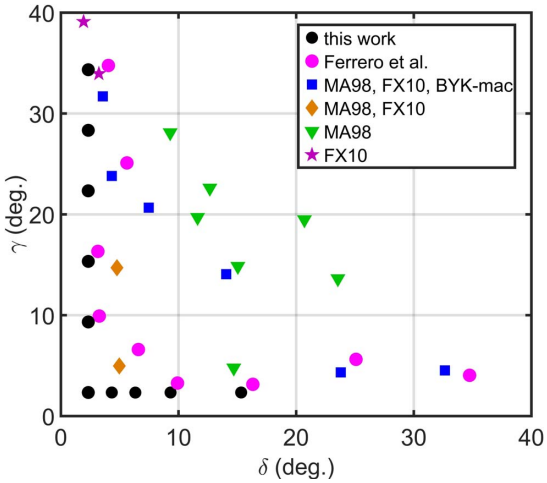

Fig. 9. Overview of the geometries proposed for the color prediction in this paper and in Ref. [18] and the measurement geometries of commercial instruments (X-Rite MA98, Datacolor FX10 and BYK-mac).

and are then turned into continuous functions of $f(\delta)$ and $g(\gamma)$ by using suitable fitting functions. This is simply done by polynomial interpolation or an exponential function for $f(\delta)$ in the case of a sparse grid (hence, $-\log(A(\delta)) \propto \delta$). Once f and g are known, an estimate of the tristimulus values for a geometry with any γ and δ can be calculated as

$$T_1 T_2 \frac{f(\delta)g(\gamma)}{g(\gamma_0)} + X_d = T_1 T_2 \frac{A(\delta)R_X(\gamma_0)A(\delta_0)R_X(\gamma)}{A(\delta_0)R_X(\gamma_0)} + X_d = X(\delta,\gamma), \quad (11)$$

wherefrom CIELAB color coordinates follow. The deviation between the measured (index m) and the predicted (index c) CIELAB color coordinates is

$$\Delta E^*_{ab} = \sqrt{(L^*_c - L^*_m)^2 + (a^*_c - a^*_m)^2 + (b^*_c - b^*_m)^2}, \quad (12)$$

where the indices refer to the geometries depicted in Fig. 4.

For all samples measured in this study, Table 2 compiles the average deviation $\langle \Delta E^*_{ab} \rangle$ and compares how this deviation is affected by the choice of the basis set. In addition, Fig. 10 shows histograms of $\langle \Delta E^*_{ab} \rangle$. With the overall mean prediction accuracy of the samples in this study being better than 4.0, the color estimation procedure is certainly sufficient to derive a fair impression of a coating's appearance. However, the accuracy is not yet sufficient to predict the color below the level of a noticeable difference.

Table 2. Accuracy of the Predictions by Eq. (11)[a]

	Sparse Sampling	Dense Sampling			
Sample	$\langle \Delta E^*_{ab} \rangle$	$\langle \Delta E^*_{ab} \rangle$	σ_L	σ_a	σ_b
CF	2.6	1.9	0.8	1.4	1.1
MB	3.9	2.6	1.5	1.5	1.9
LS	5.8	5.6	1.5	2.6	3.8
SH	2.8	1.9	1.6	0.1	0.2
VF	4.8	3.8	1.5	1.9	2.0
SR	2.9	2.5	0.8	0.7	0.4

[a]Dense sampling refers to a total of 70 basis geometries and sparse sampling to 10.

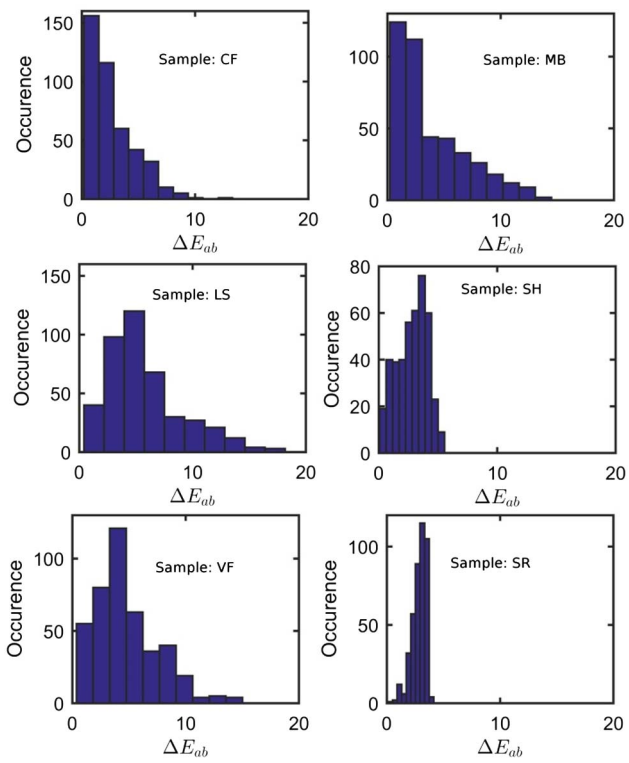

Fig. 10. Histograms of the deviation ΔE^*_{ab} between the measured color coordinates (at the geometries depicted in Fig. 5) and the ones estimated based on the sparse grid in Fig. 8.

Figure 11 illustrates the color deviation in dependence of the geometry and points out how different the prediction accuracy is depending on the type of the pigment. Especially the samples LS and VF, which contain so-called Colorstream pigments, show comparably large deviations. The deviation is strongest for inclination angles δ of about 20° and large flake incidence angles, i.e., in geometries where there are very few but still some pigments with a matching inclination angle and where the lateral distance the light travels in the layer is not small compared to the vertical distance. These are thus geometries where both scattering and the specular reflection on the pigments play an important role and this intermediate regime is not yet very well described by the model.

It can be seen that the accuracy of the prediction suffers slightly when the size of the basis set is reduced. On average the accuracy is reduced by 30% when the size of the basis set is reduced to 10 (from 70). So there is possibly some room for improvement when better ways to fit $f(\delta)$ and $g(\gamma)$, and thus essentially the curves in Fig. 8, can be found. Refining the underlying model in Eqs. (5) and (6) may also contribute to a further significant enhancement of the accuracy. For instance, potential improvement may be achieved by a more realistic model of the scattered, diffuse contribution to the appearance [26] and also by regarding effects associated with reflection on more than one pigment or shadowing. However, there is a lower limit of the accuracy which can be eventually achieved because in reality the sample appearance is not fully rotationally

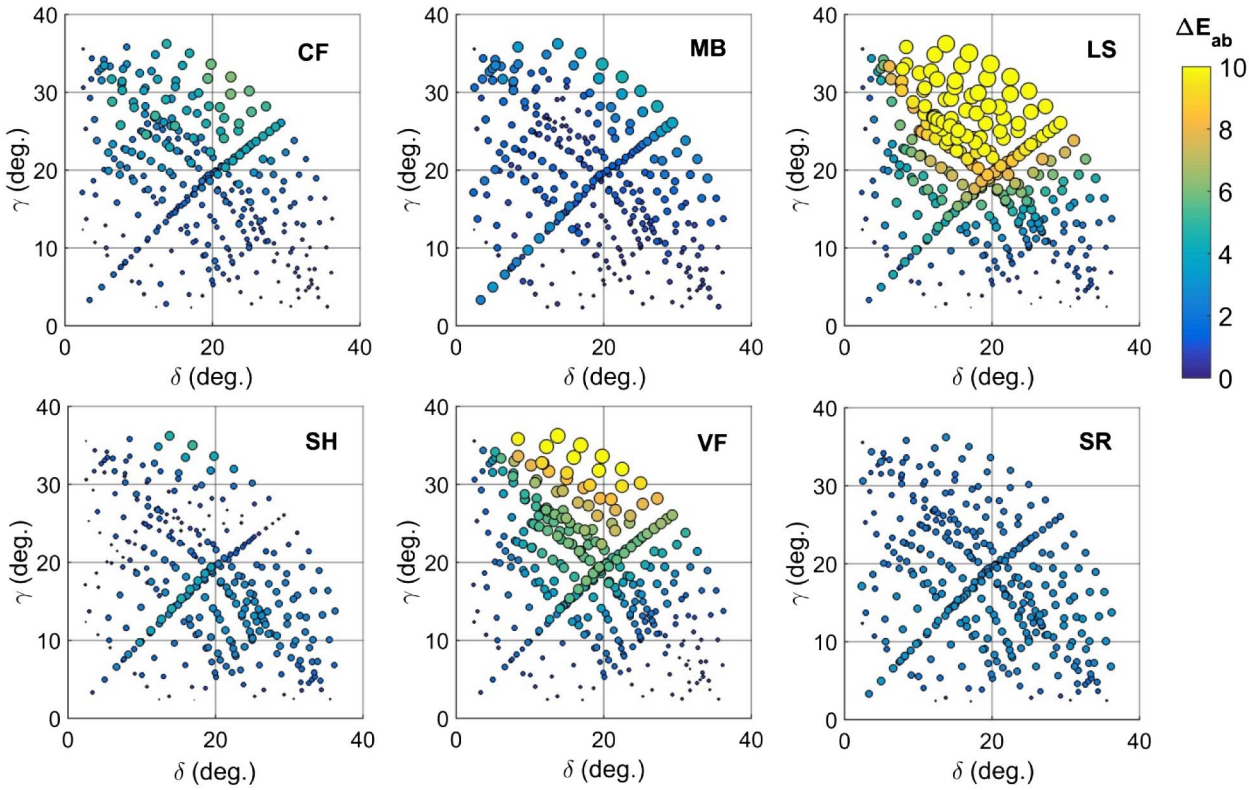

Fig. 11. Deviation ΔE^*_{ab} between the measured and predicted CIELAB color coordinates in dependence of the inclination angle δ and the incidence angle γ. The deviation is illustrated by both area and color of the markers, where any color deviation bigger than 10 units has the same color.

symmetrical around the surface normal [25]. For instance, rotating sample LS (with the worst prediction accuracy) around its normal at perpendicular incidence and $\theta_o = 20°$, which means that δ and γ remain unaltered, leads to a color difference of $\Delta E_{ab} = 3.8$. The amount of prediction uncertainty that stems from the sample anisotropy cannot be eliminated without an evaluation of the anisotropy through measurements. However, anisotropy is rather a task that should be addressed in the manufacturing step and so far the accuracy of the color prediction is already at least as good as the accuracy of the methodology in Refs. [15] and [18].

6. CONCLUSIONS

In this paper we present a new method to predict the appearance of effect-pigmented surfaces for any illumination and observation geometry based on a set of in-plane measurements only. The method makes use of a simple physical model which relies on the assumption that the appearance of interference effect pigments depends on just two parameters: the angle of incidence on the pigment flakes and their inclination with respect to the surface normal. The accuracy of the prediction is tested for six different effect pigmented samples by determining the color differences ΔE^*_{ab}, i.e., the difference between measured and predicted colors, for more than 400 different geometries, most of them being out-of-plane geometries. If just ten in-plane geometries are used, the deviations between the predicted CIELAB color coordinates and the measured ones are typically in the lower single figure range. Hence, the proposed method is very promising to achieve the goal to characterize special effect coatings by means of a limited set of measurements. Since the underlying physical model can be modified or extended, e.g., by taking into account scattering processes, room for improvement is offered. We think that the presented method will foster further progress to accurately describe and predict the appearance of effect pigments by means of a suitably chosen set of standardized geometries.

Funding. European Commission (EC); EURAMET e.V.

Acknowledgment. This work has been realized within the European Metrology Research Programme (EMRP) project JRP-IND52. The EMRP is jointly funded by the EMRP participating countries within EURAMET and the European Union. We thank the European Commission and the EURAMET e.V. for financial support.

[†]Deceased, May 12, 2015.

REFERENCES

1. F. J. Maile, G. Pfaff, and P. Reynders, "Effect pigments—past, present and future," Prog. Org. Coat. **54**, 150–163 (2005).
2. G. Pfaff and P. Reynders, "Angle-dependent optical effects deriving from submicron structures of films and pigments," Chem. Rev. **99**, 1963–1982 (1999).
3. G. A. Klein, *Industrial Color Physics* (Springer, 2010).

4. A. C. Chadwick and R. W. Kentridge, "The perception of gloss: a review," Vis. Res. **109**(Part B), 221–235 (2015).
5. S. Berthier, *Iridescences* (Springer, 2007).
6. M. Born and E. Wolf, *Principles of Optics* (Cambridge University Press, 1999).
7. J. Dorsey, H. Rushmeier, and F. Sillion, *Digital Modeling of Material Appearance* (Elsevier, 2008).
8. M. Pharr and G. Humphreys, *Physically Based Rendering* (Elsevier, 2010).
9. "Standard test method for multiangle color measurement of interference pigments," ASTM Standard E2539-14 (ASTM International, 2014).
10. "Standard test method for multiangle color measurement of metal flake pigmented materials," ASTM Standard E2194-14 (ASTM International, 2014).
11. "Tolerances for automotive paints—part 2: goniochromatic paints," DIN Stand. 6175-22001-03 (German Institute for Standardization, 2001).
12. "Colorimetry, 3rd edition," CIE Technical Report 152004 (International Commission on Illumination, 2004).
13. M. Rösler, N. Mezger, R. Dietz, and A. Huber, "Isoline concepts to find measurement geometries for effect coatings full gonio colour characterisation," Polym. Paint Colour J. **203**, 48–54 (2013).
14. A. Ferrero, E. Perales, A. M. Rabal, J. Campos, F. M. Martínez-Verdú, E. Chorro, and A. Pons, "Color representation and interpretation of special effect coatings," J. Opt. Soc. Am. A **31**, 436–447 (2014).
15. A. Ferrero, J. Campos, E. Perales, F. M. Martinez-Verdu, I. van der Lans, and E. Kirchner, "Global color estimation of special-effect coatings from measurements by commercially available portable multiangle spectrophotometers," J. Opt. Soc. Am. A **32**, 1–11 (2015).
16. A. Ferrero, A. Maria Rabal, J. Campos, A. Pons, and M. Luisa Hernanz, "Variables separation of the spectral BRDF for better understanding color variation in special effect pigment coatings," J. Opt. Soc. Am. A **29**, 842–847 (2012).
17. E. Kirchner and W. Cramer, "Making sense of measurement geometries for multi-angle spectrophotometers," Color Res. Appl. **37**, 186–198 (2012).
18. A. Ferrero, A. Rabal, J. Campos, F. Martinez-Verdu, E. Chorro, E. Perales, A. Pons, and M. Luisa Hernanz, "Spectral BRDF-based determination of proper measurement geometries to characterize color shift of special effect coatings," J. Opt. Soc. Am. A **30**, 206–214 (2013).
19. E. Kirchner and A. Ferrero, "Isochromatic lines as extension of Helmholtz reciprocity principle for effect paints," J. Opt. Soc. Am. A **31**, 1861–1867 (2014).
20. "CIE colorimetry—Part 4: 1976 L*a*b* colour space," ISO 11664-4:2008.
21. M. D. Fairchild, *Color Appearance Models* (Wiley, 2013).
22. C. S. McCamy, "Observation and measurement of the appearance of metallic materials. Part II. Micro appearance," Color Res. Appl. **23**, 362–373 (1998).
23. A. Ferrero and S. Bayon, "The measurement of sparkle," Metrologia **52**, 317–323 (2015).
24. A. Höpe, T. Atamas, D. Hünerhoff, S. Teichert, and K.-O. Hauer, "ARGon3: "3D appearance robot-based gonioreflectometer" at PTB," Rev. Sci. Instrum. **83**, 045102 (2012).
25. E. Chorro, E. Perales, F. M. Martínez-Verdú, J. Campos, and A. Pons, "Colorimetric and spectral evaluation of the optical anisotropy of metallic and pearlescent samples," J. Mod. Opt. **56**, 1457–1465 (2009).
26. J. H. Lambert, *Photometria Sive De Mensura et Gradibus Luminis, Colorum et Umbrae* (Klett, 1760).
27. "CIE colorimetry—part 2: standard illuminants for colorimetry," ISO 11664-2:2007.